High throughput measurement algorithm of maize ear 3D phenotype based on multi-view stereo vision

Ma Qin[1,2*], Zhang Qinchuan[1], Zhu Dehai[1,2], Guo Hao[1,2], Yang Ling[1]

(1. *College of Information and Electrical Engineering, China Agricultural University, Beijing 100083, China*;
2. *Key Laboratory of Agricultural Information Acquisition Technology (Beijing), Ministry of Agriculture, Beijing 100083, China*)

Abstract: As the manual measurement of maize ears in maize precision breeding is low-efficiency, labor-intensive, big-error and difficult to measure 3D indexes (such as row number, kernel number per row, rate of kernel loss, rate of kernel mold), a multi-view stereo vision algorithm for high throughput measurement of maize ear 3D phenotype was proposed. Considering the shape of maize ear is a solid of revolution, we analyzed several methods that acquire images of maize ear in 360 degrees, such as rotating scanner method, plain mirror imaging method and transparent board method. According to our analysis, we used a drop-and-shot method (three CCD cameras crossed 120 degrees mutually) to acquire images of maize ear in all degrees. For optimizing both speed of high throughput maize ear test (reduce full image scan) and accuracy of 3D measurement, we have done the followings: 1) Constructed the regular triangle measurement model based on triangulation, epipolar geometry and a few prior knowledges and solved contradictory equations using least square method. Hence, we can acquire depth information from three cameras that crossed 120 degrees mutually, calculate the 3D coordinates of maize ears according to parallax of three views and recover the 3D phenotype information of maize ears. 2) As the surface of maize ear is curved and the edge of maize ear region is difficult to recognize, we proposed a maize ear spatial overlap model based on regular triangle measurement model to calculate the overlap parts of three views of maize ear without laser mark. The new algorithm does not need to do a lot of image scan, image fusion and image transformation, thus, it can greatly speed up the 3D measurement process. Experiments showed that the average accuracy of maize ear 3D phenotype measurement is 93.96%. Our proposed algorithm provided significant technical and methodological base for high throughput maize ear test which is of great importance for maize ear test efficiency.

Keywords: maize ear, high throughput maize ear test, 3D phenotype, multi-view stereo vision

Citation: Ma, Q., Q. C. Zhang, D. H. Zhu, H. Guo, and L. Yang. 2017. High throughput measurement algorithm of maize ear 3D phenotype based on multi-view stereo vision. International Agricultural Engineering Journal, 26(3): 356–366.

1 Introduction

Maize ear analysis is an important part of maize new varieties breeding and it has great significance for maize production and scientific research. For the maize ear's irregular shape (solid of revolution) and uneven growth, the phenotypic trait (row number, kernel number per row, bare tip rate, lack of kernels, rate of mold kernels, etc.) acquisition device of ear needs to meet the high-throughput and all-dimensional requirements. As the large-scale precision varieties breeding of maize is developing, the shortness of manual maize ear test, such as low-efficiency, labor intensive and big error, becomes more and more serious. Therefore, it is of great importance to investigate the precise measurement algorithm of maize ear 3D phenotype.

Recently, researchers investigated both measurement algorithms and measurement devices for maize ear 3D phenotype.

Hausmann et al. (2009) developed a high-throughput system for image analysis of maize which can measure the width, height, row number and kernel number per row etc. of maize ears. Pearson (2009) developed an image-based hardware using FPGA to separate grains with slight color differences which is high-speed and

Received date: 2017-06-15 **Accepted date:** 2017-09-12

* **Corresponding author: Ma Qin,** Ph.D., Associate Professor, Major in pattern recognition and image processing, College of Information and Electrical Engineering, China Agricultural University, Beijing, 100083, China. Email: sockline@163.com.

low-cost. Zhao et al. (2015) used a modified OTSU method which combines multi-threshold segmentation and RGBM gradient descent to count the kernel number with accuracy of 96.8%. Miller et al. (2017) used sliding-window Fourier transform analysis of image intensity features and Bayesian analysis of contour points to measure the traits of maize ears and kernels on them, further they validated the method by comparing it with the typical manual method. Su et al. (2017) proposed a 3D reconstruction method of potatoes based on machine vision, and used the method to measure the length, width and thickness of potatoes with a relative accuracy of 95% and an absolute error of 3 mm. Gong et al. (2015) modeled the leaves of pakchoi and then accurately measured the leaves area of pakchoi using a stereo vision system. Shao et al. (2016-1; 2016-2) proposed a PSO (particle swarm optimization) based 3D point cloud simplification algorithm and a discrete wavelet threshold based point cloud data denoising algorithm to reconstruct stored bulk grain and estimate its volume. Gage et al. (2017) developed a tassel image-based phenotyping system (TIPS) and validated the proposed system with manual measurement, further their system could measure some characteristics that cannot be measured manually, such as curvature, fractal dimension, skeleton length and perimeter.

Wang et al. (2013; 2014) proposed a three-dimensional reconstruction method of maize ear which generates the point cloud of maize ear by binocular vision. Then they validated the method by RANSAC (Random Sample Consensus) and a method of generating panoramic image of maize ear which acquires a sequence of maize ear images in different perspectives first and then stitches these images by SIFT (Scale Invariant Feature Transform) characters. A computer vision based method which measures the area, perimeter, width and height of maize kernels by watershed segmentation was developed by Wang et al. (2011). Measuring the traits of maize ear is of importance (Cao et al., 2011; Qi et al., 2011), but it is not easy for maize ear's irregular shape. Guo et al. (2007) put forward an idea about constructing three-dimensional model of maize by using prior knowledge of maize. Liu et al. (2014) proposed a method to measure the width, length, row number and kernel number per row of maize ear by rotating the maize ear and acquiring a sequence of images. This method processes one maize ear for about 102 seconds with accuracy about 95%. Ma et al. (2012) measured the 3D traits by one single image using HSV histogram segmentation algorithm. Yang et al. (2011) determined the best single character in the selected characters by using those characters to classify maize varieties with linear regression. Liu et al. (2013) generated the panoramic image of maize ear by a line scan camera and then stitched those images by cross correlation of selected template. This method counted the kernels number and kernel rows number with accuracy of 94.6% and 99.1%, respectively. Wu et al. (2013) developed an automatic test instrument for maize. The equipment processes one sample for about 20 seconds with accuracy of 97%. Han et al. (2010) proposed a machine vision based method to count maize ear rows by edge marker and discrete curvature, the absolute error and relative error of this method are 0.103% and 0.66%, respectively. Duan et al. (2014) proposed a camera calibration method for maize measurement based on binomial distribution and least square method. Liang et al. (2016) developed a novel maize kernel scorer to automatically measure 12 maize kernel traits using line-scan imaging and image processing and automatic control technique, the mean relative error of manual and automatic measurement is less than 5% while processing one maize ear for 6 seconds. Du et al. (2016) proposed a maize ear phenotyping method based on distribution map of kernels. The method captured a sequence of maize ear images by rotating the maize ear with a stepper motor and then used distortion correction method to generate a sequence of standard maize ear images. The method measured row number, kernel number, width and length of maize ear with an accuracy of 94%. Wen et al. (2016) proposed a modeling method of maize ear based on 3D point cloud. They used a 3D scanner to obtain the 3D point cloud data of maize ear and generated precise model of maize ear using about 200 seconds per maize ear.

In conclusion, most solutions of automatic maize ear 3D phenotyping used panoramic photography, image mosaic and image fusion which are complex and time-consuming, hence they cannot meet the requirement of high throughput maize ear test. In order to meet the requirement of high throughput maize ear test, we proposed a high throughput measurement algorithm of maize ear 3D phenotype based on triangulation and a few prior knowledges of maize ear, constructed regular triangle measurement model (RTMM) of maize ear, implemented depth measurement of RTMM and restored maize ear 3D phenotype. We further developed a maize ear spatial overlap model (MESOM) based on RTMM to calculate the overlap parts in three views of maize ear without laser mark and eliminate the overlap parts. Our proposed algorithm avoided a lot of images scanning, images transformation and images fusion, used RTMM and MESOM to calculate maize ear 3D phenotype. Hence, we can speed up the 3D measurement process a lot which is significant for improving the efficiency of maize ear test.

2 Materials and method

High throughput maize ear test devices need to obtain all-dimensional information of maize ear and need to be fast and precise enough at the same time. As the shape of maize ear is solid of revolution, we considered rotating scanner method, plain mirror imaging method and transparent board method. Finally, a drop-and-shot method (three CCD cameras crossed 120 degrees mutually) was adopted to acquire images of maize ear in all degrees which is shown in Figure 1. We can see in Figure 1 that our device consisted of a black box, a tube to drop maize ear, several light sources and three CCD cameras (two-megapixel cameras, three cameras crossed 120 degrees mutually to acquire images of maize ear in all degrees). As Figure 2 displayed, we called the camera at the top of Figure 2 the top camera, the camera at the left of Figure 2 the left camera and the camera at the right of Figure 2 the right camera.

Our proposed new algorithm for high throughput maize ear measurement contained the following three steps:

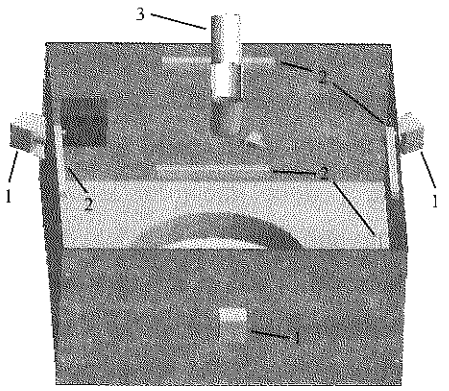

1. CCD cameras 2. Light sources 3. A tube to drop maize ear

Figure 1 Design of image acquisition device

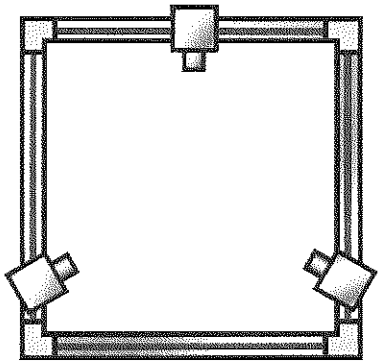

Figure 2 Distribution of cameras

1) Image acquisition and 3D calibration. Due to the non-standard distribution of cameras (three cameras distributed as a regular triangle rather than two cameras placed closely in parallel), we could not use traditional calibration method, such as Hartley algorithm and Bouguet algorithm. Thus, our algorithm calibrated three cameras pairwise and then associated three cameras by a central camera. We firstly obtained the intrinsic matrix of every camera respectively and then calculated the rotation matrix R and translation matrix T pairwise to determine the spatial relationship of three cameras.

2) Construction of RTMM of maize ear. We constructed our RTMM using triangulation and a few prior knowledges, measured depth information of spatial points using epipolar geometry and least square method solving contradictory equations, calculated spatial coordinate of maize ear using parallax of three views of maize ear so that we can measure maize ear 3D phenotype.

3) Construction of MESOM. As the surface of maize ear is curved surface and the edge region of maize ear in every view is difficult to recognition, we constructed MESOM based on RTMM to the overlap parts in three views without laser mark and eliminate the overlap parts.

2.1 Camera 3D calibration

3D calibration needs to correct error brought by manufacturing and installing our device, although three cameras crossed 120 degrees mutually in theory.

We performed 3D calibration by the following three steps.

Step 1: We used a 9*6 white and black chessboard as calibration object and applied Zhengyou Zhang's calibration method to calibrate every single camera. Zhang's calibration method obtained intrinsic and extrinsic parameters of camera by calculating several homography matrices of white and black chessboard in different poses. Figure 3 was the white and black chessboard we used, Figure 4 was the result of corner recognition of the chessboard and Figure 5 displayed the calibration result of single camera.

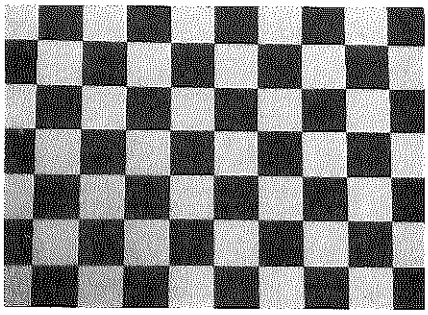

Figure 3 White and black chessboard

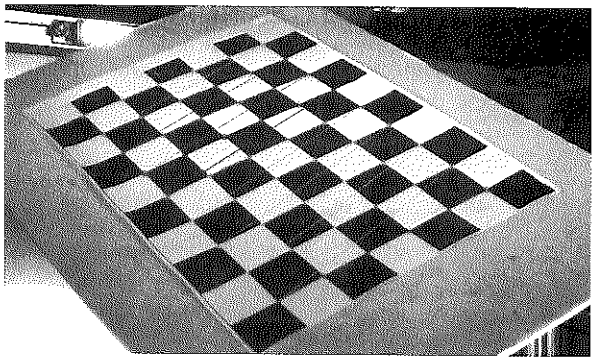

Figure 4 Corner recognition

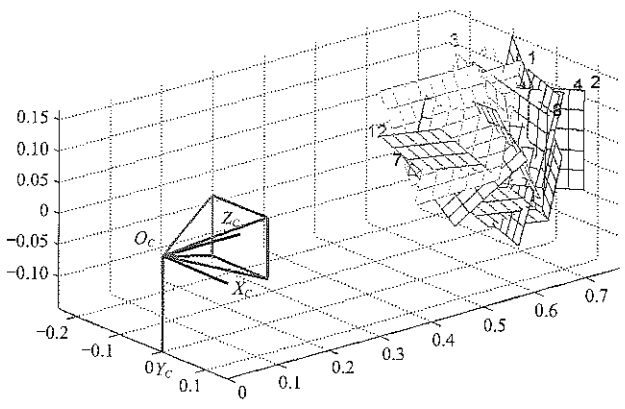

Figure 5 Calibration of single camera

Step 2: In order to calculate the rotation matrix R and translation matrix T between two cameras, we calculated the extrinsic parameters of two cameras respectively as Formula (1), where P_1 is the coordinate of point P in left camera system, P_r is the coordinate of point P in right camera system, R_l is the rotation matrix of left camera, R_r is the rotation matrix of right camera, T_l is the translation vector of left camera, T_r is the translation vector of right camera, P is the coordinate of point P in object system.

$$\begin{cases} P_l = R_l P + T_l \\ P_r = R_r P + T_r \end{cases} \tag{1}$$

Two cameras can be associated by a rotation matrix R and a translation vector T as Formula (2) showed.

$$P_l = R^T(P_r - T) \tag{2}$$

Combined formulas (1) and (2), we can reduce Formula (3) to calculate R and T.

$$\begin{cases} R = R_r(R_l)T \\ T = T_r - RT_l \end{cases} \tag{3}$$

Extrinsic parameters of every single camera can be calculated by Zhengyou Zhang's calibration method. And then we can solve R and T by substituting the extrinsic parameters to Formula (3).

Step 3: To make sure that optical axes of two cameras are in parallel and in the same direction, we can decompose rotation matrix R into r_1 and r_2, use these matrices to rotate images of two cameras to one plane. Further, to align the lines in two images, we have to calculate an alignment matrix R_{rect} which maps the polar point of one camera to infinity.

We calibrated three cameras pairwise and associated three cameras by a central camera. Figure 6 displayed two views of the same object captured by two cameras. Figure 7 displayed the simulation result of 3D calibration of two cameras which claimed that the accuracy of our algorithm is reasonably high.

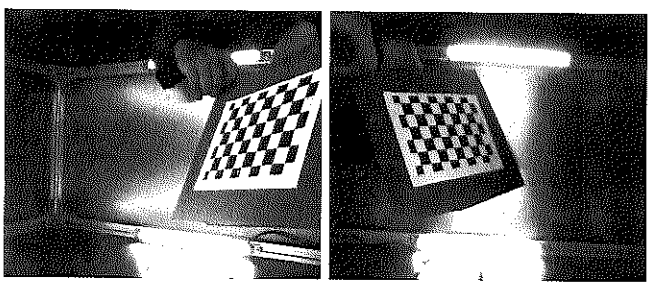

Figure 6 Views of two cameras

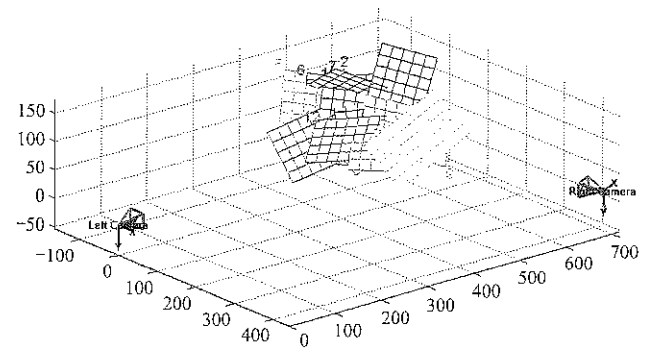

Figure 7 3D calibration of two cameras

2.2 Construction of RTMM of maize ear

We can extract the contour of dropping ear in image by frame difference method. The result is shown in Figure 8.

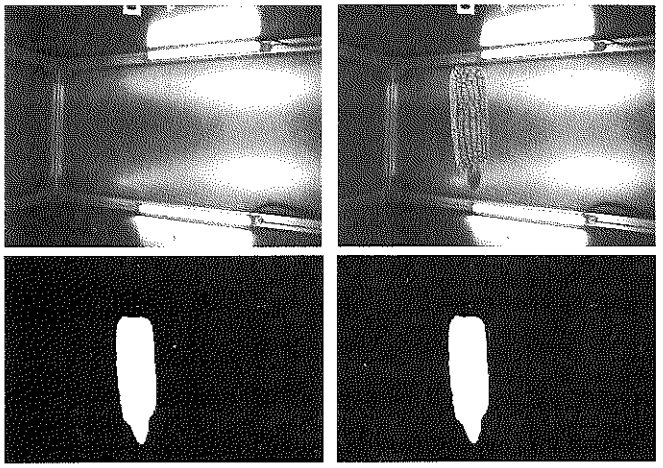

Figure 8 Contour extraction of dropping ear by frame difference method

2.2.1 Epipolar geometry and solve intersection of spatial lines

An observation point in the image plane is corresponded to infinite points in the three-dimensional space. These points are located on the line connecting camera shooting origin and observation point. In this paper, left-camera coordinate system is chosen as world coordinate system, so camera shooting origin O_l is coordinate origin. The task is to calculate Z coordinate value in world coordinate system for three-dimensional space observation point P, which also means the depth information is in front of the camera.

Let the coordinate of P be (X, Y, Z) and let the coordinate of P_l be (x_l, y_l, f_l). P_l is the observation point in left-camera image plane of P. Then, the parametric equation of spatial line is as follows:

$$P = t_l P_l \tag{4}$$

where, t_l is parameter need to calculate, coordinate value of P can be expressed as $(t_l x_l, t_l y_l, t_l f_l)$.

In the same way, set right-camera coordinate system as current coordinate system and give parametric equation of spatial line between P and the observation point in right-camera image plane of P, P_r. But two equations are not in the same coordinate system, it is necessary to convert P_r to world coordinate system firstly. The Formula is expressed as:

$$P_r' = R^T P_r + T \tag{5}$$

where, R and T are the rotation matrix and translation matrix between left-camera and right-camera calculated in 2.1.

Meanwhile, obtain the coordinate value of word coordinate system for the right-camera shooting origin O_r, the value is T. So the parametric equation of spatial line $O_r P_r$ is as follows:

$$P = T + t_r(P_r' - T) = t_r R^T P_r + T \tag{6}$$

Then, according to Formulas (4) and (6), the new Formula is as following:

$$t_l P_l = t_r R^T P_r + T \tag{7}$$

Solve the equations could calculate parameters t_l and t_r, then it is easy to compute the depth information of P. But in the actual measurement process exists camera noise and other measurement errors, it causes that the two spatial lines are non-co-planar and then the equations are contradictory equations. In 2.3.2, use other method to solve the equations.

We can calculate depth information for every two cameras of those three cameras and take advantage of their mean to correct each other so that we can obtain a more accurate result.

2.2.2 Solve contradictory equations

Solve the Equations (7) to calculate the intersection of spatial line, but in actual measurement process the equations are contradictory equations sometimes, that is the two straight lines of actually solving progress may be non-co-planar, the reasons are as follows:

Image noise and accuracy of extract contour, it causes the corresponding points-pairs we selected is not the corresponding points-pairs of actual environment

The errors of calibration progress

The Formula (7) is summarized as:

$$At = T \tag{8}$$

where, A is one 2×3 matrix; t is the 2-dimensional vector needs to solve. The Equations (8) may be contradictory equations because the number of equations are more than variables. Define residual δ of the equations as follow:

$$\delta_i = \sum_{j=1}^{2} a_{ij} t_j - T_i,\ i = 1,2,3 \tag{9}$$

The current task is to solve $t=[t_1, t_2]^T$ and make sure the residual δ is minimum. Define vector $e=[\delta_1, \delta_2, \delta_3]^T$ and judge magnitude of residual by e. This algorithm use minimal 2-norm method

$$\|e\|_2 = \left(\sum_{i=1}^{3} \delta_i^2\right)^{\frac{1}{2}} = \left\{\sum_{i=1}^{3}\left[\sum_{j=1}^{2} a_{ij} t_j - T_i\right]^2\right\}^{\frac{1}{2}} \tag{10}$$

Define two-variables function $Q(t_1, t_2) = \sum_{i=1}^{3} \delta_i^2$, then the problem of solving minimal 2-norm can be converted to the problem of solving the minimum point of the function. For the minimum point of multivariate function, the value of the partial derivative is zero, just like:

$$\begin{bmatrix} \frac{\partial Q}{\partial t_1} \\ \frac{\partial Q}{\partial t_2} \end{bmatrix} = 2\begin{bmatrix} a_{11} & a_{21} & a_{31} \\ a_{12} & a_{22} & a_{32} \end{bmatrix}\begin{bmatrix} \sum_{j=1}^{2} a_{1j} t_j - T_1 \\ \sum_{j=1}^{2} a_{2j} t_j - T_2 \\ \sum_{j=1}^{2} a_{3j} t_j - T_3 \end{bmatrix} = \begin{bmatrix} 0 \\ 0 \end{bmatrix} \tag{11}$$

The Formula (11) can be formed $2A^T(AT-T)=0$. Then form to regular linear equations, the final form is:

$$A^T A t = A^T T \tag{12}$$

The solution of this equation is the least square solution of the original contradictory equations. The solution is the unique solution of the original equations when the value of minimum of residual is zero. So solve Equations (12) to instead of solving the original contradictory equations.

2.2.3 Convert image pixel coordinates to image physical coordinates

Before calculate the depth information of the observation point using Formula (12), it is necessary to convert image pixel coordinates of image coordinate system to image physical coordinates of camera coordinate system.

It is achieved by intrinsic parameter matrix of camera to convent coordinate from camera physical coordinate system to image coordinate system. How can the method convent point from image coordinate system to image physical coordinate system is as the following:

$$p = M^{-1} q \tag{13}$$

where, p is the coordinate of image physical coordinate system; q is coordinate of image coordinate system; M is the intrinsic parameter matrix of camera.

2.3 Maize ear spatial overlap model

Overlapping parts exist when three cameras acquire the dropping maize ears, so it is necessary to remove the overlapping part to prepare for phenotype measurement next step.

2.3.1 Locate position of maize ear

Before calculate the overlap parts of maize ear, we have to locate the maize ear. Hence, we need to select two prior points that are easy to find in three views of maize ear. Our algorithm selected midpoint and quartile as such points. We can calculate the spatial coordinate of midpoint (so is quartile) so that we can locate the maize ear:

Step 1. Calculate the minimum enclosing rectangles of maize ear in three views.

Step 2. Calculate the center points of the minimum enclosing rectangles in three views.

Step 3. Use RTMM to calculate the spatial coordinate of midpoint.

2.3.2 Calculate the overlapping parts

The next task is to calculate the overlapping parts of maize ear when three cameras acquire the image of dropping maize ear, the overlapping parts are only necessary to calculate once.

First some prior facts are as follows:

The angle between optic axis of two cameras is not accurate 120°, this angle needs to calculate by calibration because of the hardware equipment errors.

The center of maize ear is hard to fall the equidistant position of three cameras. The distance from the point to three cameras should be calculated by RTMM in actual environment.

The center of maize ear is not at the center axis of image because of irregular position of ear, so this model could not be established by nature of center axis.

As it is shown in Figure 9, the maize ear is almost dropping vertically because of hardware equipment. The observation plane of maize ear can be considered as a circle approximately. Define O_{top}, O_{left} and O_{right} as the shooting centers of top, left and right camera. Define T_1,

T_2, L_1, L_2, R_1, R_2 as the edge points of maize ear observed by clockwise. It is easy to find arc T_1L_2, arc R_1T_2 and arc L_1R_2 are the overlapping parts of ear.

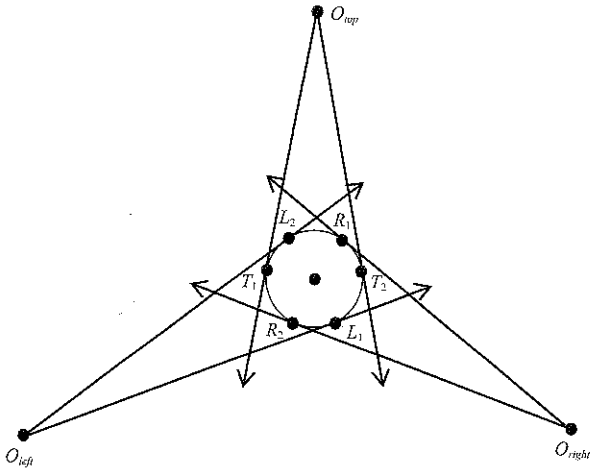

Figure 9 Schematic diagram of spatial overlap region

Then the task is to calculate coordinate of these points. The coordinate calculation method of three cameras is consistent, take the top camera as an example, the calculation model is shown in Figure 10.

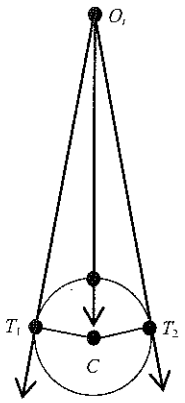

Figure 10 Calculation model of tangency for top-camera

where, T_1, T_2 are tangency of circle C, the radius value is half of ear diameter. The coordinate of point C is calculated by RTMM, so it is easy to calculate the length of tangent O_tT_1 and O_tT_2 by Pythagorean theorem.

Set the coordinate of point C as (x_c, y_c, z_c), the length of two tangents as l, the radius of circle as r, then the plane equation of circle C is:

$$(x-x_c)^2+(z-z_c)^2=r^2 \tag{14}$$

At the same time, the distance from O_t to tangency is:

$$x^2+z^2=l^2 \tag{15}$$

The coordinate of T_1 and T_2 can be computed by Formula (14) and Formula (15). Set $a=l^2+x_c^2+z_c^2-r^2$ and the coordinate of T_1 and T_2 can be expressed as:

$$\begin{cases} x_1=\dfrac{3a-\sqrt{a^2+2l^2x_c^2}}{4x_c} \\ z_1=\dfrac{-a+\sqrt{a^2+2l^2x_c^2}}{4z_c} \end{cases}, \quad \begin{cases} x_2=\dfrac{3a+\sqrt{a^2+2l^2x_c^2}}{4x_c} \\ z_2=\dfrac{-a-\sqrt{a^2+2l^2x_c^2}}{4z_c} \end{cases} \tag{16}$$

The coordinate that computed is based on own camera coordinate system, convent the coordinate to corresponding camera coordinate system by Formula $P'=R^TP+T$, the matrix R and T are computed in camera calibration process in the preceding paragraphs.

After these calculation steps for every camera of three, the coordinate of four points about overlapping parts of every camera are calculate achieved. Then remove overlapping parts unnecessary to calculate for three cameras by some rules. In this paper, the rule is only to calculate clockwise direction overlapping parts for every camera, anti-clockwise direction overlapping parts is calculated for the camera anti-clockwise direction to current camera.

2.4 Calculate row number and grain number of maize ear

2.4.1 Choose calculation region of row number

The kernels located at the edge of maize ear image are hardly to observe clearly due to projection deformation, so it is necessary to remove the edge area while calculating row number. For the overlapping parts of three cameras, the row number may be counted twice, so remove these areas to improve precision.

In this paper, cut maize ear image before compute row number, the cutting methods are as follows:

Remove the head and tail of the ear, only left the center area of maize ear (the length half of ear length).

Remove the area that does not need to calculate by Maize ear spatial overlap model.

Choose 80% of residual width region in right align as final counting region.

The schematic diagram of region selection is shown in Figure 11.

2.4.2 Kernel contour extraction

In this paper, use the maize ear contour calculate in the above as mask at first, then separate G color channel of maize ear image and extract kernel contour by OTSU threshold method, as shown in Figure 12.

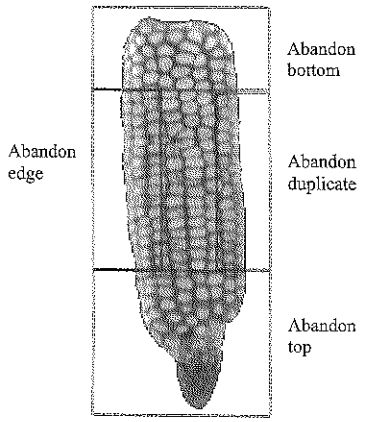

Figure 11 The schematic diagram of row number region selection

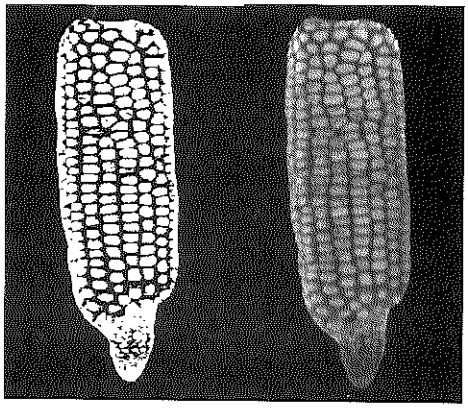

Figure 12 Contour extraction of kernels

2.4.3 Row number calculation of main area

The grains located in middle position of maize ear are regular arrangement relatively, row number at main area is shown in Figure 13. As Figure 13 shows, the image is alternatively composed of the kernel area and the kernel joint area. The kernel area has more white pixel point and the kernel joint area contains more black pixel point. In this paper, use the statistical Formula (17)

$$p_i = \sum_{j=1}^{y} f(i,j),\ i = 1,2,3,...,x \qquad (17)$$

where, $f(i, j)$ is pixel value for the point which located at (i, j) coordinate of the image. The pixel value of white pixel point and black pixel point are 0, 1 respectively. x and y are width and height of main area.

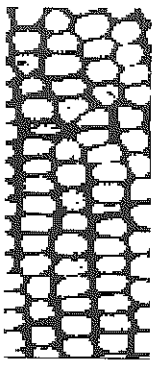

Figure 13 Main area to count row number

Use Formula (17) to count for each column of the image, then a statistical graph is obtained. The statistical graph is shown in Figure 14, it seems like wave line. The wave crest in the graph is kernel area and wave trough is kernel joint area. So the number of wave crest is row number in main area. It is contained 5 wave crests in this image and the row number in actual image is 5.

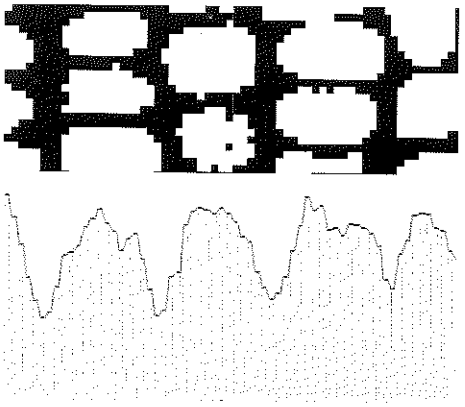

Figure 14 The statistical graph of row number

2.4.4 Row number calculation of edge region

The errors are big when do row number calculation of edge region, so in this paper, edge region proportion model (ERPM) is established to calculate kernel of edge region. The schematic diagram of ERPM is shown in Figure 15.

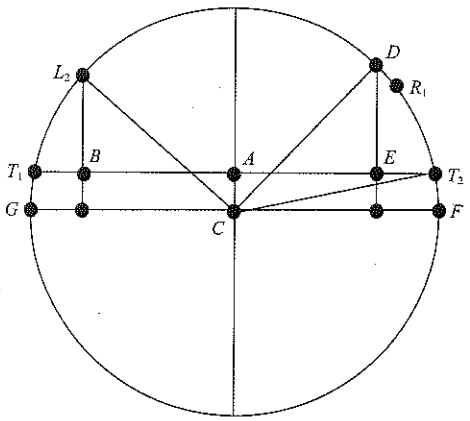

Figure 15 Schematic diagram of ERPM

Set top camera as current camera, T_1T_2 is the maximum width top camera acquired. Arc L_2D is main area and arc DT_2 is the edge region. The coordinate of circle center C is known, so the sinusoidal value of $\angle T_2CF$ is $\frac{r}{l}$, l is the distance between C to origin point. The cosine value of $\angle T_2CF$ is $\frac{AT_2}{r}$. So the length of AT_2 is

$$AT_2 = a = \frac{r}{l}\sqrt{l^2 - r^2} \tag{18}$$

Then the length of AE, ET_2, and AB can be calculated by ration. Set $E=b$, $AB=c$, $\angle T_2CF=\theta$, $\angle T_2CD=\gamma$, $\angle T_2CP=\varphi$, then these formulas can be derived

$$\begin{cases} \theta = \arcsin\dfrac{r}{l} \\ \gamma = \arccos\dfrac{b}{r} - \theta \\ \varphi = \dfrac{\pi}{2} + \arccos\dfrac{c}{r} - \gamma - \theta \end{cases} \tag{19}$$

The ratio between γ and φ is equal to the ratio between main area arc L_2D and edge region arc DT_2. Then the row number of edge region can be calculated by the ratio and the row number of main area.

Each camera can get the number of rows in the area it is in charge of and after which it is calculated after the number of rows in the main area and the number of rows in the edge region. Due to the overlapping area before processing, the information of the number of rows that are processed by the three views will not be repeated, that is to say, the results of the number of rows per row in the final three views should be:

$$r = r_{top} + r_{left} + r_{right} \tag{20}$$

It must be noted that the number of rows here is a floating point number while the actual number of rows should be even, so the statistical results should be even to the nearest integer.

According to the statistical method of row number, the same method can be applied to the number of parameters, statistical calculation of X axis pixel accumulation, which can avoid the interference of a small number of grains or defects effectively.

3 Results and discussion

Take 10 ears of maize, and collect three views of the images at the same time, total 30 data, and the center of gravity for the extraction of ear contour correspondence, which to solve the problem of the RTMM, the distances between maize ear center and three camera centers respectively. Compared with manual measurement, the average accuracy of our proposed algorithm is 93.96% which is shown in Table 1.

We further use our proposed algorithm to calculate the row number and kernel number per row, which can verify that our measurement of row number and kernel number per row is also feasible. The analysis of row number and kernel number per row of the above 10 samples is as shown in Table 2 and Table 3.

Table 1 Table of accuracy analysis of RTMM

Camera	Average error	Minimum error	Maximum error	Standard deviation
Top	6.24%	2.62%	9.51%	0.018
Left	5.96%	2.34%	8.97%	0.021
Right	5.92%	3.94%	7.87%	0.014

Table 2 Results for row number

Index	1	2	3	4	5	6	7	8	9	10
Manual	16	18	18	14	16	18	18	16	18	16
Paper Method	16	18	18	14	16	16	18	16	18	16

Table 3 Results for kernel number per row

Index	1	2	3	4	5	6	7	8	9	10
Manual	27.67	28.33	31.67	30.33	29	30.33	33.33	30.67	29.33	30
Paper Method	28.56	27.44	33.13	31.76	30.99	28.38	32.54	29.17	28.66	31.73

In Table 3, the actual number of rows is measured by the number of lines of the main three rows and then the average number of lines. It can be concluded according to the data from table that, the zero-error rate of the measurement of row number is 100% and the measurement error of the kernel number per row is less than 2.

4 Conclusion

As manual measurement in maize precision breeding is low-efficiency, labor-intensive and difficult to measure 3D phenotype (row number, kernel number per row, rate of kernel loss and rate of kernel mold), we developed a new high throughput measurement algorithm of maize ear 3D phenotype based on multi-view stereo vision. For both high throughput maize test speed and precise 3D measurement, we have done the followings:

1) We analyzed standard structure of binocular vision whose optical axes of cameras are parallel. Then we developed our RTMM of maize ear. We constructed our model using triangulation and a few prior knowledges, measured depth information of spatial points by epipolar geometry and solving contradictory equations using least square method and calculated spatial coordinate of maize ear by parallax.

2) The edge parts of maize ear in every view is difficult to recognize because the surface of maize ear is curved. To solve this problem, we proposed a MESOM model based on RTMM to calculate the overlap parts in three views of maize ear and eliminate the overlap parts without laser mark. We combined RTMM and MESOM to measure maize ear 3D phenotype which avoided a lot of image scanning, image fusion and image transformation and speeded up 3D measurement a lot.

3) Our algorithm had 93.96% average accuracy in 3D measurement, 100% accuracy in maize ear row number measurement and error less than 2 in measuring kernel number per row.

Our algorithm provided important technical and methodological base for high throughput maize ear test which is significant for improving efficiency of maize ear test.

Acknowledgements

We would like to thank to the reviewers for their helpful comments. This work was financially supported by the Chinese Universities Scientific Fund (#2017XD002) and the Special Fund for Agro-scientific Research in the Public Interest (#201203026).

[References]

[1] Cao, J. H., Y. Z. Ran, and J. C. Guo. 2011. The design and realization of corn test system. *Journal of Changchun Normal University*, 30(4): 38–41.

[2] Du, J. J., X. Guo, C. Wang, and B. Xiao. 2016. Computation method of phenotypic parameters based on distribution map of kernels for corn ears. *Transactions of the Chinese Society of Agricultural Engineering*, 32(13): 168–176. (in Chinese with English abstract).

[3] Duan, X. C., J. H. Zhou, and S. J. Wang. 2014. Image calibration method for the ear of corn measurement system. *Journal of Agricultural Mechanization Research*, 36(1): 76–79.

[4] Gage, J. L., N. D. Miller, E. P. Spalding, S. M. Kaeppler, and D. N Leon. 2017. TIPS: a system for automated image-based phenotyping of maize tassels. *Plant Methods*, 13(1): 21.

[5] Gong, L., R. Chen, Y. S. Zhao and C. L. Liu. 2015. Model-based in-situ measurement of pakchoi leaf area. *International Journal of Agricultural and Biological Engineering*, 8(4): 35–42.

[6] Guo, X. Y., C. J. Zhao, Y. Liu, X. Y. Qin, X. Y. Deng, and G.Y.Sun. 2007. Three-dimensional visualization of maize based on growth models. *Transactions of the Chinese Society of Agricultural Engineering*, 23(3): 121–125. (in Chinese with English abstract).

[7] Han, Z. Z., and J. Z. Yang. 2010. Vision research on the machine of counting ear rows in maize. *Journal of Maize Sciences*, 18(2): 146–148, 152.

[8] Hausmann, N. J., T. E. Abdaie, and C, Mark. 2009. Method and system for digital image analysis of maize: US. WO2009023110(A1).

[9] Liang, X. Y., K. Wang, C. L. Huang, X. H. Zhang, J. B. Yan, and W. N. Yang. 2016. A high-throughput maize kernel traits scorer based on line-scan imaging. *Measurement*, 90: 453–460.

[10] Liu, C. Q., and B. Q. Chen. 2014. Method of image detection for ear of corn based on computer vision. *Transactions of the Chinese Society of Agricultural Engineering*, 30(6): 131–138. (in Chinese with English abstract).

[11] Liu, G. Y., X. H. Yang, M. Bai, and H. Li. 2013. Detecting techniques of maize ear characters based on line scan image. *Transactions of the Chinese Society for Agricultural Machinery*, 44(11): 276–280. (in Chinese with English abstract).

[12] Ma, Q., J. T. Jiang, D. H. Zhu, S. M. Li, S. L. Mei, and Y. C. Liu. 2012. Rapid measurement for 3D geometric features of maize ear based on image processing. *Transactions of the Chinese Society of Agricultural Engineering*, 28(Supp.2): 208–212. (in Chinese with English abstract).

[13] Miller, N. D., N. J. Haase, J. Lee, S. M. Kaeppler, N. de Leon, and E. P. Spalding. 2017. A robust, high-throughput method for computing maize ear, cob, and kernel attributes automatically from images. *Plant Journal for Cell and Molecular Biology*, 89(1): 169–178.

[14] Pearson, T. 2009. Hardware-based image processing for high-speed inspection of grains. *Computers and Electronics in Agriculture*, 69(1): 12–18.

[15] Qi, J. T., S. H. Zhang, X. T. Niu, and Y. Xu. 2011. Design and application of yield monitor system for corn ear. *Transactions of the Chinese Society for Agricultural Machinery*, 42(1): 181–185. (in Chinese with English abstract).

[16] Shao, Q., T. Xu, T. Yoshino, Y. J. Zhao, and W. T. Yang. 2016. Point cloud simplification algorithm based on particle swarm optimization for online measurement of stored bulk grain. *International Journal of Agricultural and Biological Engineering*, 9(1): 71–78.

[17] Shao, Q., T. Xu, T. Yoshino, N. Song, and H. Zhu. 2016. Classified denoising method for laser point cloud data of stored grain bulk surface based on discrete wavelet threshold.

International Journal of Agricultural and Biological Engineering, 9(4): 123–131.

[18] Su, Q. H., N. Kondo, M. Li, H. Sun, and D. F. A. Riza. 2017. Potato feature prediction based on machine vision and 3D model rebuilding. *Computers and Electronics in Agriculture*, 137(C): 41–51.

[19] Wang, C. Y., X.Y. Guo, W. L. Wen, and T. Miao. 2011. The measurement of maize kernel shape based on computer vision. *Journal of Agricultural Mechanization Research*, 33(6): 141–144.

[20] Wang, C.Y., X.Y. Guo, S. Wu, B. Xiao, and J. Du. 2013. Investigate maize ear traits using machine vision with panoramic photography. *Transactions of the Chinese Society of Agricultural Engineering*, 29(24): 155–162. (in Chinese with English abstract).

[21] Wang, C. Y., X. Y. Guo, S. Wu, B. Xiao, and J. Du. 2014. Three dimensional reconstruction of maize ear based on computer vision. *Transactions of the Chinese Society of Agricultural Machinery*, 45(9): 274–279. (in Chinese with English abstract).

[22] Wen, W.L., Y. Wang, T. Y. Xu, T. Yang, and X. Guo. 2016. Geometric modeling of maize ear based on three-dimensional point cloud. *Journal of Agricultural Science and Technology*, 18(5): 88–93.

[23] Wu, J. W., X. Y. Guo, and C. Y. Wang. 2013. Automatic test instrument for maize test. *China Seed Industry*, 9: 51–52.

[24] Yang, J. Z., H. S. Zhang, J. P. Hao, T. Q. Du, F. Z. Cui, N. N. Li, and G. M. Liang. 2011. Identifying maize cultivars by single characteristics of ears using image analysis. *Transactions of the Chinese Society of Agricultural Engineering*, 27(1): 196–200. (in Chinese with English abstract).

[25] Zhao, M.M., J. Qin, S. M. Li, Z. Liu, J. Cao, X. H. Yao, S. J. Ye, and L. Li. 2015. An automatic counting method of maize ear grain based on image processing. *Computer and Computing Technologies in Agriculture VIII*, 452: 521–533.